IEEE Access
Multidisciplinary | Rapid Review | Open Access Journal

Received October 8, 2021, accepted December 5, 2021, date of publication December 15, 2021, date of current version December 29, 2021.

Digital Object Identifier 10.1109/ACCESS.2021.3135959

Design and Application of a Nitrate Measurement System Based on a Narrowband Tunable Ultraviolet Light Source

XINGYUE ZHU[1], KAIXIONG YU[1], XIAOFAN ZHU[1], AND CHI WU[1,2,3]

[1]Shandong Provincial Center for in-situ Marine Sensors, Institute of Marine Science and Technology, Shandong University, Qingdao 266237, China
[2]Aixsensor Company Ltd., Dezhou 253000, China
[3]Southern Marine Science and Engineering Guangdong Laboratory, Guangzhou 511458, China

Corresponding author: Chi Wu (qi.wu@sdu.edu.cn)

This work was supported in part by the China Postdoctoral Science Foundation under Grant 2019M662365, in part by the Shandong Provincial Natural Science Foundation under Grant ZR2020QD086, in part by the Key Technology Research and Development Program of Shandong under Grant 2019JZZY020711 and Grant 2018YFJH0702, in part by the State Key Research and Development Project of China under Grant 2019YFC1408600, and in part by the Qingdao Postdoctoral Applied Research Project.

ABSTRACT The nitrate concentration in seawater is an important parameter for marine environment monitoring, which is of great significance for the analysis of seawater ecosystems. In this paper, a novel nitrate measurement system based on a narrowband tunable ultraviolet light source and support vector regression (SVR)-based algorithm is proposed and demonstrated. The system is composed of a tunable light source module, an optical fiber splitter, a temperature control module, a spectrometer and a data processing module. By controlling the motorized rotation stage and motorized filter wheel, a continuous and automatic narrowband tunable deep ultraviolet (DUV) light source module is developed. Different seawater samples from Aoshan Bay (Qingdao, China), the Western Pacific, Sanggou Bay (Weihai, China) and the South China Sea with nitrate concentrations of 0-102 μmol/L are measured by this system based on a narrowband tunable DUV light source and the results are compared with those of a broadband DUV light source system. The calculation model is established based on the SVR algorithm with/without temperature and salinity correction (TSC), and the prediction results are compared with those of the in situ ultraviolet spectrophotometry (ISUS) algorithm. The results show that the method based on a narrowband tunable light source system and the TSC-SVR algorithm has the best performance in predicting the nitrate concentration, where the root mean squared error (RMSE) decreased by 29.16% (from 1.20 to 0.85 μmol/L) compared with the results of the broadband light source system, and the error range is from -3.01 to 2.99 μmol/L. The proposed method in this paper has the potential to provide more accurate measurements in marine environment monitoring.

INDEX TERMS Nitrate sensor, narrowband tunable light source, ultraviolet spectrophotometry, SVR algorithm, spectral correction.

I. INTRODUCTION

Real-time and accurate measurement of nitrate concentrations is of great significance for marine ecosystem research and marine water quality assessment [1]. Currently, in situ nitrate monitoring has become a trend in marine environmental research. Therefore, it is necessary to develop a rapid and in situ technology to monitor the nitrate concentration in seawater with high accuracy.

The methods for in situ nitrate measurements include the wet chemical method and ultraviolet spectrophotometry method. In the research process of wet chemical methods, flow injection analysis (FIA) was first proposed by Ruzicka and Henson, which greatly promoted the development of automatic online monitoring instruments [2], [3]. Afterwards, analytical in situ nitrate instruments were developed [4]. In recent years, microfluidic chip technology has been developed in the field of water quality detection due to its advantages of low power consumption, high sensitivity and rapid analysis, this technology can detect trace nitrate

The associate editor coordinating the review of this manuscript and approving it for publication was Chao Zuo.

TABLE 1. Comparison of the proposed system with existing state-of-the-art methods.

Technology	Representative product	Application	Characteristics
Wet chemical method	YSI EXO2	River water, ground water, seawater	The ion selective electrode will clearly drift after a period of time. The consumption rate and effective working time of the chemical reagent limits its long-term application.
Ultraviolet spectrophotometry method	SUNA/ISUS/SUV-6	Seawater	The broadband light is used as the light source, which does not conform to Lambert-Beer's law. Usually, there is a linear or nonlinear relationship between the output of the sensors and the reference nitrate concentrations. Therefore, a further correction is needed to obtain final high accuracy values [10-11].
Proposed method	-	Seawater	The narrowband light is used as the light source, which conforms to Lambert-Beer's law. The final measurement result can be obtained directly from the system.

concentrations [5], [6]. The ion selective electrode (ISE) method has also been commercialized for nitrate detection. For example, YSI Inc. (USA) is committed to in-situ detection of nutrients in seawater based on the ISE method [7], and its latest product, EXO2, can determine NO3-N with a detection range of 0.1-1000 mg/L, an accuracy of ± 2 mg/L and a resolution of 0.01 mg/L. Hach Company (USA) also proposed the NO3D sc nitrate sensor based on the ISE method with a range of 0.1-1000 mg/L NO3-N and a minimum detection limit of 0.5 mg/L NO3-N. However, this sensor is only suitable for clean water with relatively simple compositions. Moreover, with electrode consumption, the internal electromotive force will be decreased, which can cause measurement error. Therefore, the lifetime of an in situ sensor based on the wet chemical method depends on the consumption rate and effective working time of the chemical reagent, which limits its long-term application in underwater measurements.

The method based on ultraviolet spectrophotometry can directly measure nitrate without using chemical reagents. In 1998, Finch and his research group designed an in-situ sensor based on three wavelengths with a resolution of 0.21 μmol/L NO3- in seawater [8]. Since the temperature and salinity affect the measurement, a correction algorithm was developed for an in situ ultraviolet spectrophotometry (ISUS) system. The results showed that the standard error was two times lower than that without correction (from 1.4 down to 0.65 μM) when the sensor was tested in the Southern Ocean and Pacific Ocean [9], [10]. Afterwards, Pidcock and his colleagues developed a low-power sensor (SUV-6) using an improved algorithm and obtained a sensitivity as high as ± 0.2 μmol/L [11]. A few generations of in situ nitrate sensors were developed by Sea-bird Scientific, which could be used for various natural environments [12]–[14]. In addition, by integrating with other sensors and using salinity or pH sensors to correct the measurement data [15], [16], multiparameter sensors such as WTW UV705IQ NOx and TriOS-NICO could achieve a measurement range of 0-100 mg/L and an accuracy of $\pm(5\% + 0.1)$. However, many experimental results obtained from different water environments have revealed that the measurement errors of some commercial nitrate sensors are actually larger than the values in their product technical manuals [17], [18]. Therefore, the measurement accuracy for nitrate sensors remains a challenge today.

A comparison of the proposed system with existing state-of-the-art methods is shown in Table 1. At present, nitrate sensors based on ultraviolet spectroscopy mostly use broadband light sources, which do not conform to the monochromatic light incident requirement of Lambert-Beer's law. Moreover, the output of these sensors slightly deviates from those of the high-precision autoanalyzer and must be further calibrated against the reference concentrations to obtain final high accuracy values [11]. In recent years, the support vector regression (SVR) algorithm has shown powerful performance in the prediction of practical engineering problems due to its flexibility and easy implementation. For example, Sun et al presented a new hybrid approach of SVR and fruitfly optimization algorithms to predict scour hole geometry below ski-jump spillways. The results show that the developed hybrid model is a robust approach and improves the precision level by $\sim 8\%$ compared with the simple SVR algorithm [19]. Taghizadeh-Mehrjardi et al proposed an SVR algorithm with wavelet transformation (W-SVR) to estimate the soil salinity in arid regions. Using an uncertainty estimation based on local errors and clustering methods, W-SVR showed a better performance than SVR in predicting the soil salinity [20]. Shahaboddin et al used different machine learning-based models, including improved SVR algorithms to predict soil temperature at different depths and wave heights in coastal waters, which indicates a certain prediction ability of the

SVR algorithm in multivariate nonlinear regression analysis [21], [22]. Therefore, to optimize the measurement technology based on the existing ultraviolet spectrophotometry method (including making such measurements consistent with Lambert-Beer's law and directly obtaining more accurate results), a nitrate measurement system based on a narrowband tunable ultraviolet light source with a temperature and salinity correction (TSC)-based SVR algorithm is first proposed and demonstrated in this manuscript. The results are compared and analyzed to verify the feasibility of the system with a narrowband light source, which lays the foundation for nitrate sensor optimization.

II. THEORY

A. WAVELENGTH-TUNABLE PRINCIPLE BASED ON A MULTILAYER INTERFERENCE FILTER

For a multilayer thin film filter, the optical path difference is fixed between each layer. According to equivalent theory, the multilayer film can be simplified to a single-layer film with a transfer matrix, as shown in figure 1. Assume that the equivalent refractive index and thickness of the thin film filter are N and h, respectively. When the light is incident on the upper surface 1 of the filter from air (refractive index n_0) with incident angle θ, partial light is refracted into the filter with refraction angle θ_1. Then, the light continues propagating with partial light reflected to upper surface 1 and partial light emitted from bottom surface 2 [23].

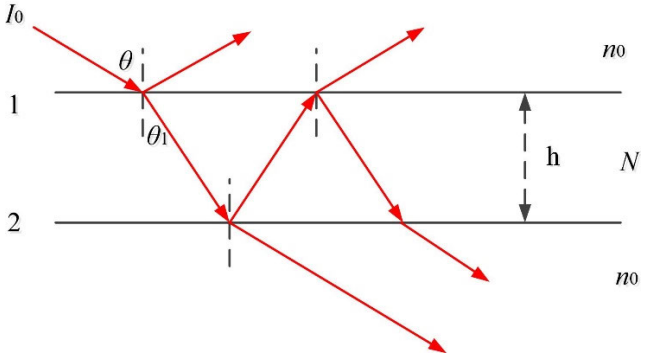

FIGURE 1. Principle of multi-beam interference.

In this case, the optical path difference Δ and phase difference δ of two transmitted beams can be expressed as follows [24]:

$$\Delta = \mathbf{2Nh}\cos\theta_1 \tag{1}$$

$$\delta = 2\pi\Delta/\lambda = 4\pi Nhcos\theta_1/\lambda \tag{2}$$

When the light is normally incident to surface 1 ($\theta = \theta_1 = 0$), the central wavelength of the transmitted light is λ_0. The phase difference of the interference light can be expressed as [25]:

$$\delta = 4\pi Nh\cos 0/\lambda_0 = 4\pi Nhcos\theta_1/\lambda \tag{3}$$

Based on Snell's law, we have [26]:

$$n_0 sin\theta = Nsin\theta_1 \tag{4}$$

Finally, the central wavelength λ of the transmitted light can be calculated as [27]

$$\lambda = \lambda_0\sqrt{1 - (n_0 sin\theta/N)^2} \tag{5}$$

Equation (5) is the relationship between central wavelength λ and incident angle θ when the incident light is oblique. For a filter with known λ_0, the central wavelength of the transmitted light is only related to the incident angle. Therefore, by changing the incident angle, the central wavelength of the transmitted light can be tuned in a certain range to realize a narrowband tunable light source.

B. ABSORBANCE PRINCIPLE

Lambert-Beer's law is the basic law to establish the relationship between an absorption spectrum and the analyte concentration. Absorbance A_λ of the measured sample at each wavelength λ can be expressed as [10]:

$$A_\lambda = -log_{10}\left\{(I_\lambda - I_D)/\left(I_{\lambda,0} - I_D\right)\right\} \tag{6}$$

where I_λ is the light intensity out from the sample, $I_{\lambda,0}$ is the light intensity out from the deionized water, and I_D is the dark current of the detector. A higher nitrate concentration corresponds to a greater decrease in light intensity and a larger absorbance is. Therefore, the nitrate calculation model can be established based on different seawater absorbance A_λ values.

III. MATERIAL AND METHODS

A. MEASUREMENT SYSTEM DESCRIPTION

1) STRUCTURE OF THE SYSTEM

The measurement system is designed based on photoelectric sensor technology and spectral analysis technology. The system structure is shown in figure 2, which is mainly composed of a narrowband tunable light source module, a signal acquisition module and a data processing module.

The narrowband tunable light source module is made by splitting the broadband ultraviolet spectrum through interference filters. One of the slots on the filter wheel is empty, which can allow broadband light to pass through. The signal acquisition module includes a collimating lens, sample cells, a beam-splitting fiber, a temperature control module, temperature and salinity sensors and a spectrometer. The beam-splitting fiber is used to monitor the light signal in real time and reduce the influence of light fluctuations. The seawater sample is in sample cell 1 (12 in figure 2), and the deionized water is in sample cell 2 (13 in figure 2). The temperature and salinity sensors are in sample cell 2 to collect data for the calculation model. The optical path of the underwater reflection probe is fixed at 10 mm. An ultraviolet spectrometer (QE Pro, Ocean Optics Inc., USA) was used to collect the measurement data. The data processing module includes model establishment, absorbance calculation and data analysis. The specifications of the system are shown in Table 2.

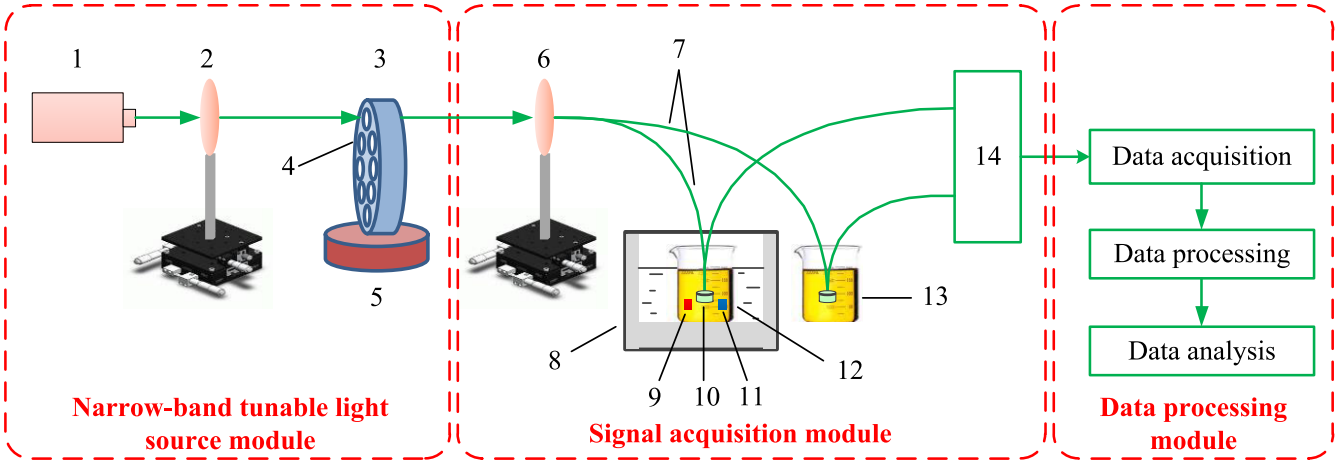

FIGURE 2. Structure of the measurement system. 1-Deuterium lamp (DH-2000, Ocean Optics Inc., USA); 2, 6-collimating lens; 3-motorized filter wheel (with12 filter slots, Edmund optics Inc., USA); 4-ultraviolet interference filters; 5-motorized rotation stage (URS100bpp, Newport Corp., USA); 7-ultraviolet fiber splitter (customized, Wyoptics Co., Ltd., China); 8-temperature control module; 9-temperature sensor; 10-reflection probe; 11-salinity sensor; 12-sample cell 1; 13-sample cell 2; 14-ultraviolet spectrometer.

TABLE 2. Specifications of the system.

light source	
type	Deuterium lamp (DH-2000-DUV)
power consumption	585 μW
lifetime	1000 h
output wavelength	190 nm - 400 nm
output stability	less than 5×10^{-6} peak to peak (0.1-10.0 Hz)
output drift	less than 0.01% per hour
ultraviolet filters	
central wavelength	220 nm, 228 nm, 239 nm, 250 nm, 260 nm, 270 nm
diameter	12.5 mm
FWHM (full width at half maximum)	10 nm
temperature control module	
temperature range	-5 °C - 100 °C
temperature precision	0.05 °C
ultraviolet spectrometer	
wavelength range	200 nm – 385 nm
optical resolution	0.4 nm
entrance slit	10 μm
grating	GRATING_#H48
dark noise	2.5 counts RMS
signal to noise ratio	1000:1 (single acquisition)
thermal stability	0.01 pixels/°C

2) DESIGN OF THE NARROWBAND TUNABLE ULTRAVIOLET LIGHT SOURCE MODULE

The light source module is one of the core structures of the system, which includes a deuterium lamp, a collimator lens, a filter wheel, a rotation stage and several ultraviolet filters with different central wavelengths that are placed in the filter slots. A motor with a limit is used to control the filter wheel to realize the switching of the filter slots. A stepper motor is used to control the angle rotation stage to tune the light incidence angle so that the central wavelength of each filter can be continuously tuned in a certain range [28].

To accurately collect the real-time data at each wavelength, the visual software interface is established based on the C++ and QT Creator 5.9 interface framework, and the RS232 protocol is used to communicate with the angle rotation stage, filter wheel and spectrometer. The flow chart of software control is shown in figure 3. By controlling the interface, the filter position and serial ports are initialized, so that the angle of the rotation stage and the filter position will be set at their initial positions. The delay timer is used after each rotation angle of the rotation stage or after the filter wheel reaches the target position. The program determines whether the next data acquisition step is required by determining the position of the angle rotation stage and the filter wheel to ensure the accuracy of the measurement data.

B. DATA ACQUISITION METHOD

After the deuterium lamp is preheated, the dark noise of the system is first collected by the spectrometer. Afterwards, a thermostatic water bath was used to make the sample at a constant temperature. The temperature and salinity of the sample were recorded by temperature and salinity sensors, and the spectral data were collected by an ultraviolet spectrometer. The visual software interface is used to communicate with the spectrometer in real time. For each measurement, 6 filters with different central wavelengths must be replaced, and the spectral data are recorded and stored by the host computer once the filter turns to each different angle.

C. DATA PROCESSING METHOD

1) SPECTRAL CORRECTION METHOD

a: PREPROCESSING OF THE SPECTRAL DATA BASED ON A NARROWBAND TUNABLE LIGHT SOURCE

The preprocessing flow chart of the measured data is shown in figure 4. After the light passes through the filter, it is necessary to determine the transmitted wavelength of each filter at different angles. Therefore, the intensity data of

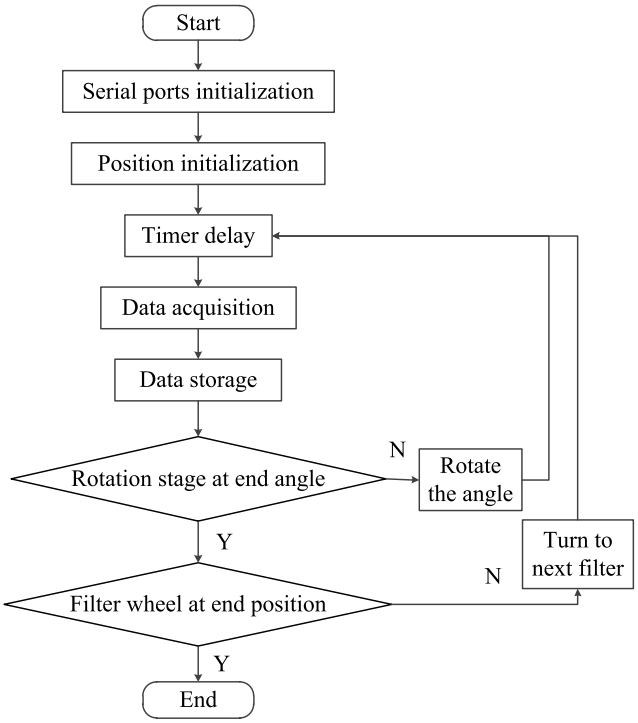

FIGURE 3. Flow chart of the software control.

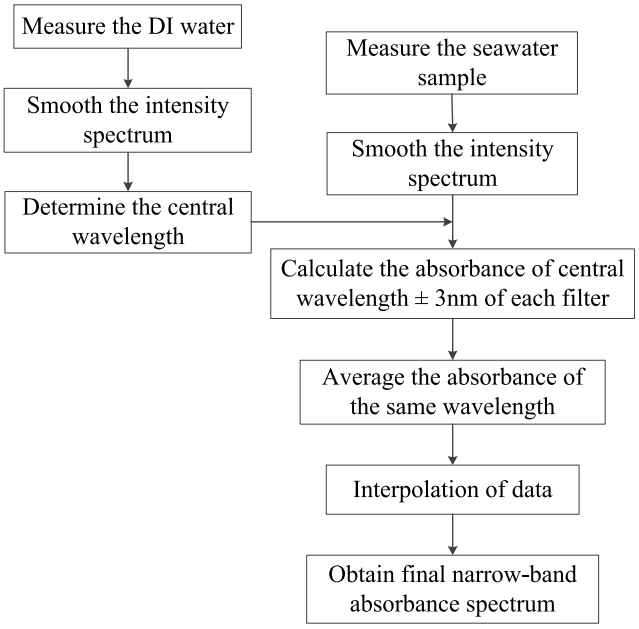

FIGURE 4. Preprocessing flow chart of the measurement data.

deionized water are measured and smoothed by the moving average (MA) method to determine the central wavelength of each filter at different rotation angles. Afterwards, the intensity spectrum of the seawater samples is measured and smoothed. To obtain more data points to smooth the absorbance spectrum, the absorbance of the central wavelength ±3 nm of each filter at different rotation angles is calculated. Afterwards, the absorbance corresponding to the same wavelength is averaged. Using the interpolation method, the wavelengths of the narrowband spectrum could be identical to those of the broadband spectrum, and the final narrowband absorbance spectrum was obtained.

b: TEMPERATURE AND SALINITY CORRECTION (TSC) ALGORITHM

The seawater absorbance will be affected by temperature and salinity [29]. Therefore, the TSC algorithm was established according to a previous study [10]. First, the low nutrient seawater (LNS, filtered Western Pacific seawater) absorbance was normalized to a salinity of 35. Based on the polynomial regression equation, the absorbance model of LNS in the range of the deep ultraviolet (DUV) spectrum can be established, and the LNS absorbance ($A_{SS}(\lambda, T, S)$) due to the temperature effect at different salinities can be calculated. Hence, the influence of temperature on absorbance can be subtracted from the measured seawater absorbance, that is [30]:

$$A' = A_{Meas} - A_{SS} \tag{7}$$

where A_{Meas} is the absorbance of the seawater samples. However, the TSC-corrected data (A') still show an offset due to chromophoric dissolved organic matter (CDOM). Therefore, a linear regression of absorption versus wavelength of 240-270 nm is subtracted from A', that is [16]:

$$\mathrm{A}'' = \mathrm{A}' - (e + f \times \lambda) \tag{8}$$

where e and f are the regression parameters. Finally, the SVR regression algorithm can be used to establish the nitrate calculation model.

2) SUPPORT VECTOR REGRESSION (SVR) ALGORITHM

SVR is a machine learning algorithm based on statistical learning theory that can properly handle nonlinear regression and has the characteristics of global optimization [31]–[33]. The established method of the SVR algorithm is briefly described as follows. Suppose that $\{(x_1, y_1), \ldots, (x_i, y_i), \ldots, (x_l, y_l)\} \in R^n \times R$ is the training sample set, where x_i is the input data, y_i is the output data, and $\mathrm{i} = 1, \ldots, \mathrm{l}$. $\mathrm{y} = f(x)$ is the estimated output value. Then, the optimal linear regression equation can be expressed as [34]:

$$y = w \cdot \varphi(x) + b \tag{9}$$

where '·' denotes the inner product, $\varphi(\cdot)$ denotes the nonlinear transformation, and b is the offset. The relaxation factors ξ_i and ξ_i^* are introduced, and y can be transformed into the following optimization problem [35]:

$$\begin{cases} \min\left(\|w\|^2/2\right) + C\sum_{i=1}^{l}\left(\xi_i + \xi_i^*\right) \\ \text{s.t} \begin{cases} y_i - w \cdot \varphi(x_i) - b \le \varepsilon + \xi_i \\ -y_i + w \cdot \varphi(x_i) + b \le \varepsilon + \xi_i^* \\ \xi_i, \xi_i^* \ge 0 \end{cases} \end{cases} \tag{10}$$

where C is the constant coefficient, $C > 0$, and ε is the insensitive loss function. The optimization problem in (10) can be solved by constructing a dual problem. Therefore, the Lagrange function with dual variables is established as follows [35]:

$$\begin{aligned} \mathrm{L}\left(w, b, \xi_i, \xi_i^*\right) = \|w\|^2/2 + C\sum_{i=1}^{N}\left(\xi_i + \xi_i^*\right) \\ - \sum_{i=1}^{N} a_i\left(\varepsilon + \xi_i + y_i - w\cdot\varphi\left(x_i\right) - b\right) \\ - \sum_{i=1}^{N} a_i^*\left(\varepsilon + \xi_i^* + y_i - w\cdot\varphi\left(x_i\right) - b\right) \\ - \sum_{i=1}^{N}\left(\eta_i\xi_i + \eta_i^*\xi_i^*\right) \end{aligned} \tag{11}$$

where $a_i, a_i^*, \eta_i, \eta_i^* \geq 0$ are Lagrange operators, and the partial derivatives of w, b,ξ_i, ξ_i^* should be 0. Finally, according to the inner product kernel defined by the Mercer theory, the regression model of SVR can be established as [35]:

$$\begin{aligned} \mathrm{y} &= \sum_{i=1}^{l}\left(a_i - a_i^*\right)\left[\varphi\left(x\right)\cdot\varphi\left(x_i\right)\right] + b \\ &= \sum_{i=1}^{l}\left(a_i - a_i^*\right)K\left(x, x_i\right) + b \end{aligned} \tag{12}$$

where $K\left(x, x_i\right)$ is the kernel function. The kernel functions mainly include the linear kernel function, polynomial kernel function, radial basis kernel function and sigmoid kernel function. Different learning machines can be constructed with different kernel functions [36]. In this paper, the radial basis kernel function is used, which can be expressed as [37]:

$$K\left(x, x_i\right) = \exp\left\{-\|x - x_i\|^2/\left(2\sigma^2\right)\right\} \tag{13}$$

where σ is the width of the kernel function.

Coefficient C, kernel function parameter σ and insensitive loss function ε are three important parameters in the SVR model. ε determines the support vector number and generalization performance. σ reflects the width of the function; a smaller σ corresponds to a more selective function. C is used to control the model complexity, and the fitting correlation coefficient increases with increasing C [38]. Some results show that the measurement accuracy first increases with the increase in C and subsequently decreases when C exceeds a certain value. Moreover, with increasing C, the support vector number at the boundary will gradually decrease until 0 [39].

3) SVR-BASED NITRATE CALCULATION MODEL

a: LIBSVM TOOL LIBRARY

LibSVM is an easy-to-use and effective support vector machine (SVM) software package developed by Dr. Lin of Taiwan University [40]. The software has the advantages of less parameter adjustment, open source code and easy expansion, and provides a cross-validation function. Currently, it has become one of the most widely used SVM tool libraries [41]–[43]. Therefore, LibSVM is used in this paper to establish the calculation model.

TABLE 3. Parameters used for SVR model.

Parameter	Value
s (SVM type)	3 (e-SVR)
t (kernel)	2 (RBF)
c	440
g	1.2
p	0.01

b: SVR-BASED MODEL ESTABLISHMENT

It has been proven that the calculation model with wavelengths of 217-260 nm can accurately predict the nitrate concentration [10]. Therefore, six bandpass filters with central wavelengths of 220 nm, 228 nm, 239 nm, 250 nm, 260 nm and 270 nm (Edmund Optics Inc., USA) are used to achieve wavelengths from 212 nm to 270 nm. The establishment process of the nitrate model based on SVR is shown in figure 5. After data collection, the spectral data are preprocessed by the method introduced in section 1.1. The size of each obtained spectral data is 1×304. TSC correction is performed on the obtained spectral data, and absorbance data of 212-240 nm with a size of 1×142 are selected as the input of the SVR model.

When the radial basis function (RBF) is used as the kernel function in the SVR model, two parameters must be determined: cost (c) and gamma (g). The cost c influences the generalization ability of the model, and gamma affects the distribution of data in high-dimensional space after RBF mapping. At present, there is no recognized optimal parameter selection method. Therefore, based on the empirical value, c and g are initialized in a certain range and continuously adjusted. By selecting the SVR model with the minimum root mean squared error (RMSE) and maximum coefficient of determination (R^2), the parameters can be determined and the calculation model is finally established. The calculation formula of RMSE and R^2 can be written as follows [30]:

$$\mathrm{RMSE} = \sqrt{\sum_{i=1}^{n}\left(y_i - y_{i,p}\right)^2} \tag{14}$$

$$R^2 = 1 - \sum_{i=1}^{n}\left(y_i - y_{i,p}\right)^2 / \sum_{i=1}^{n}\left(y_i - \hat{y}\right)^2 \tag{15}$$

where y_i and $y_{i,p}$ are the reference and predicted concentrations of the samples, respectively; $\hat{y}$ is the mean value of the reference concentration; n is the sample number. Generally, a smaller RMSE corresponds to better model performance. The final parameters for SVR and its kernel are shown in Table 3.

D. MEASUREMENT METHOD

(1) A measurement system based on a narrowband tunable ultraviolet light source was established. The relationship between the incident angles and the central wavelengths of each filter was calibrated.

(2) The seawater of Aoshan Bay (Qingdao, China), Western Pacific, South China Sea and Sanggou Bay (Weihai, China) was filtered using a 0.4 μm filter membrane.

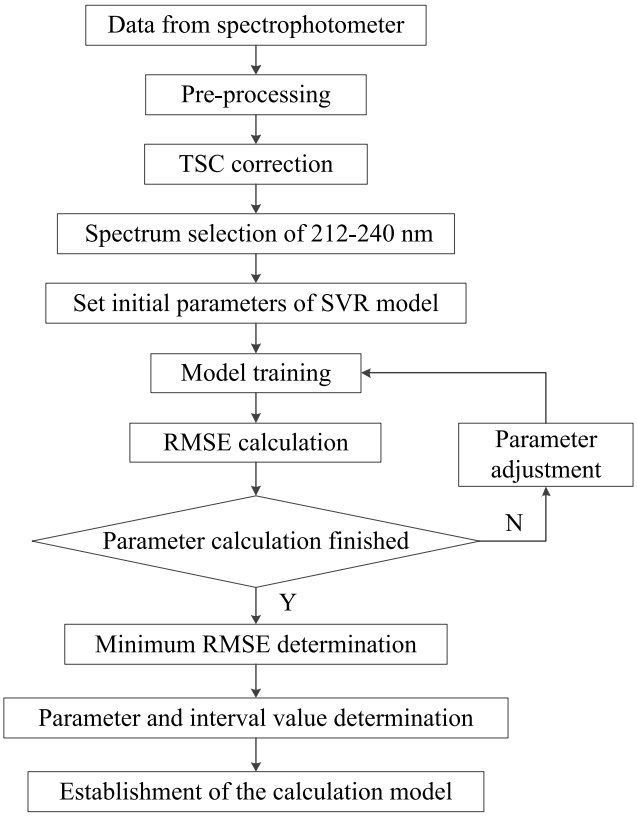

FIGURE 5. Establishment process of nitrate calculation model based on SVR.

AutoAnalyzer 3 (SEAL, Germany) was used to measure the background nitrate concentration in these seawater samples. The background nitrate concentrations are 1.99 μmol/L and 8.00 μmol/L in Aoshan Bay seawater and Sanggou Bay seawater, respectively. For the seawater of the Western Pacific and South China Sea, the nitrate concentrations are less than 0.1 μmol/L. Afterwards, different amounts of standard nitrate (0-100 μmol/L) were added to make seawater samples. All of these samples were frozen at -20 °C in clean high-density polyethylene bottles.

(3) The seawater sample data were measured at different temperatures (4-25 °C at 1 °C intervals) by systems based on broadband light source and narrowband tunable light source. The wavelength range of the nitrate calculation model was selected, and the TSC algorithm was established based on Western Pacific seawater data.

(4) A nitrate calculation model based on the SVR algorithm was established, and the measurement data of the systems based on broadband light source and narrowband tunable light source were compared and analyzed.

IV. RESULTS AND ANALYSIS

A. PERFORMANCE OF THE NARROWBAND TUNABLE LIGHT SOURCE

At the initial operation of the rotation stage, it cannot be guaranteed that the light is normally incident onto the filter. Therefore, it is necessary to calibrate the relationship between the angle of the rotation stage and the central wavelength of the transmitted light. Based on (5), the angle versus wavelength model for each filter can be calculated as:

$$f(x) = a\sqrt{1 - \{b\sin[\pi(x-c)/180]\}^2} \tag{16}$$

where a is the central wavelength of the filter with normal incidence, b is the value of n_0/N, x is the angle in the angle rotation stage, and parameter c compensates for the initial angle position. Therefore, $(x - c)$ is the incident angle of each filter. The measurement results of these filters are shown in figure 6, where (a)-(c) and (g)-(i) show the relationships between rotation angle and transmitted central wavelengths of the filters, and (b)-(f) and (j)-(l) show the intensity spectra at different rotation angles of the filters.

Figure 6 shows that with increasing incident angle, the central wavelength of the transmitted light moves to a short wavelength. Considering the minimum effective wavelength of the 220 nm filter, spectral data of 212-270 nm are selected for modeling and calculation. The parameters in (16) are shown in Table 4. The results show that the experimental data and theoretical data fit well with R^2 values larger than 0.999.

TABLE 4. Modeling parameters of each filter.

Parameter	a	b	c	R^2
220nm	221.991	0.463	3.069	0.99963
228nm	230.103	0.486	4.501	0.99963
239nm	240.776	0.521	5.148	0.99972
250nm	251.773	0.388	2.298	0.99929
260nm	262.042	0.546	7.062	0.99959
270nm	271.232	0.526	5.167	0.99974

B. NARROWBAND SPECTRUM PRE-PROCESSING RESULTS

The narrowband spectrum data are processed by the MA method and interpolation method. The preprocessing spectrum and original spectrum of Aoshan Bay seawater are compared in figure 7, where (a) is the absorbance calculated from the original intensity data, and (b) is the absorbance spectrum after the data preprocessing. In figure 7, the trend of the preprocessing spectrum is consistent with the original spectrum, and the influence of noise is reduced. Therefore, the preprocessing of the data is necessary for model establishment and data calculation.

C. TEMPERATURE INFLUENCE

The absorbance changes in the sodium bromide solution (0.8 mmol/L), sodium nitrate solution (30 μmol/L) and seawater from Aoshan Bay (Qingdao, China), the Western Pacific, Sanggou Bay (Weihai, China), and the South China Sea were measured in the temperature range of 4-25 °C with a gradient of 1 °C. The measurement results at 217 nm are shown in figure 8.

Figure 8 shows that seawater absorbance is strongly temperature-dependent because bromide absorbance is temperature-sensitive [10], [44], [45]. However, nitrate

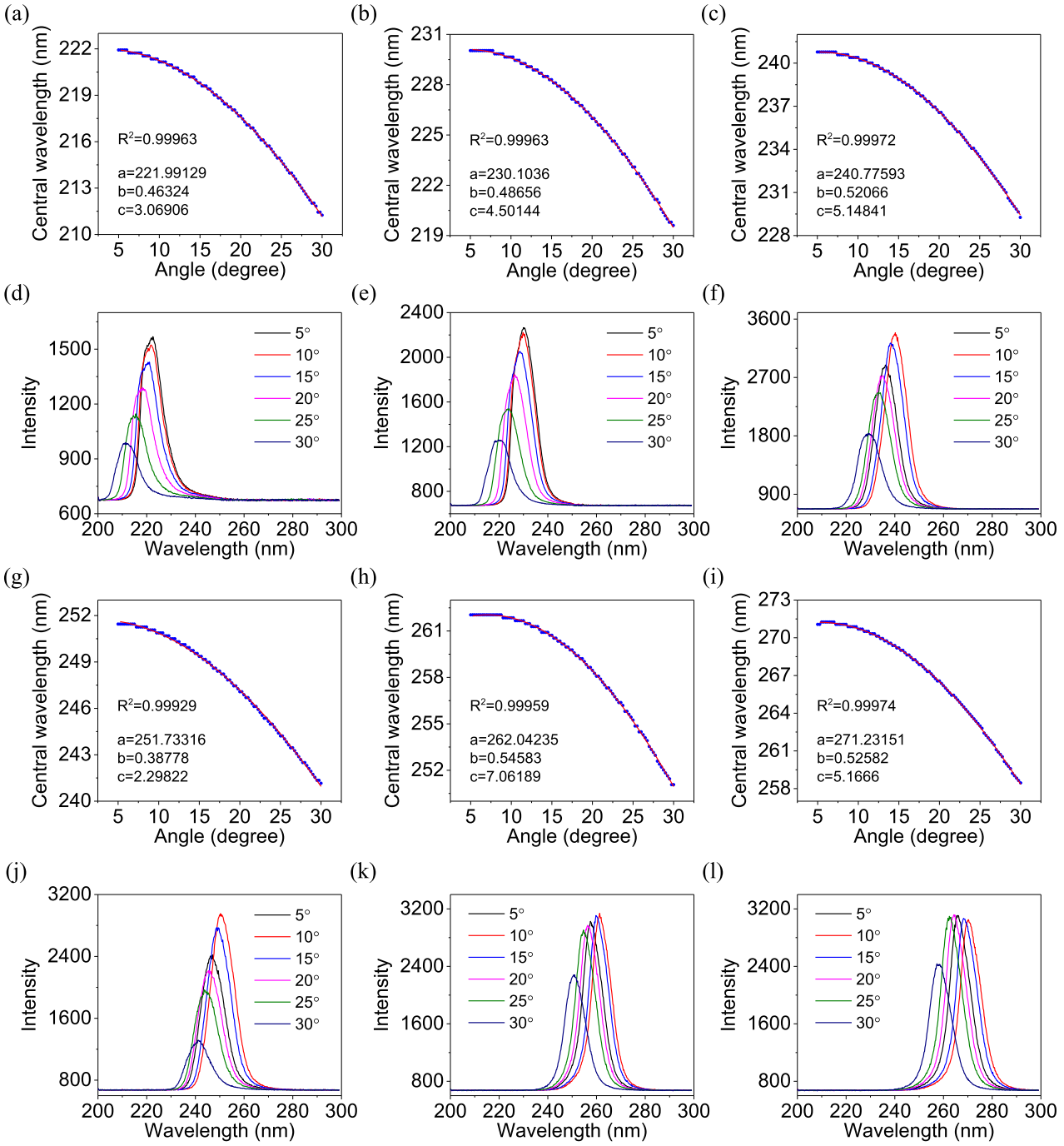

FIGURE 6. Calibration results of different filters. (a)-(c) Relationship between the rotation angles and the transmitted central wavelengths for the 220 nm, 228 nm and 239 nm filters, respectively; (d)-(f) intensity spectrum at different rotation angles for the 220 nm, 228 nm and 239 nm filters respectively; (g)-(i) relationship between the rotation angles and the central wavelengths for the 250 nm, 260 nm and 270 nm filters respectively; (j)-(l) intensity spectrum at different rotation angles for the 250 nm, 260 nm and 270 nm filters respectively.

absorption is caused by the $\pi \rightarrow \pi^*$ transition within the molecule in the ultraviolet band, so the absorbance of the nitrate solution does not obviously change with temperature [46]. As bromide is conserved with salinity, the bromide concentration is reported as a source of salinity [47], [48]. To remove the influence of temperature and salinity, TSC models are established based on LNS (filtered Western Pacific seawater) data measured by a narrowband tunable light source system and broadband light source system, respectively. The parameters are shown in Table 5, which shows no significant difference between these two TSC models.

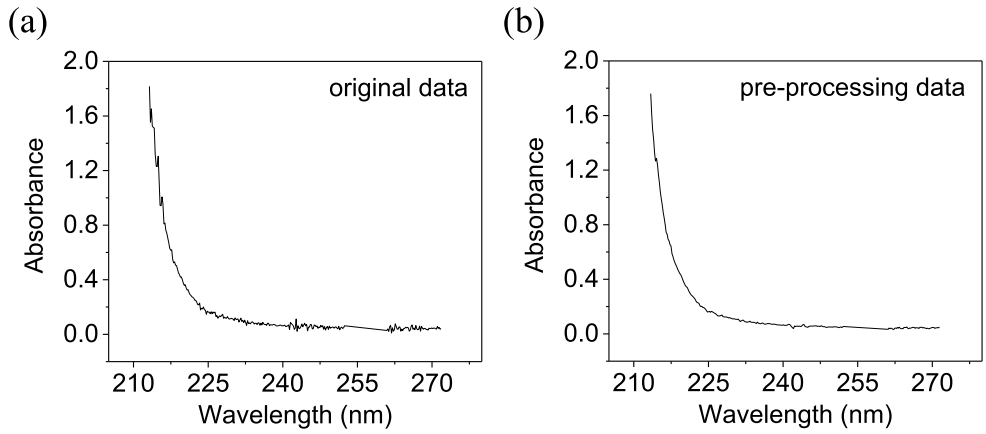

FIGURE 7. Comparison of the original spectrum and preprocessing spectrum.

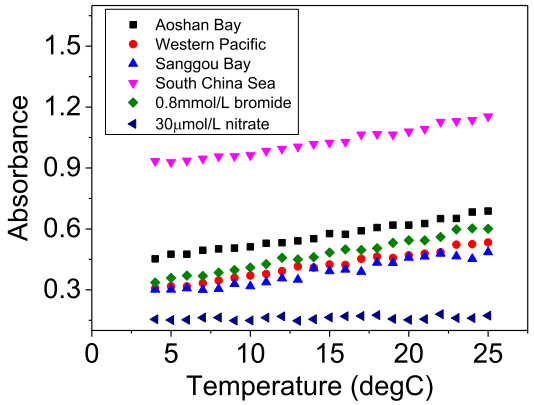

FIGURE 8. Relationship between temperature and absorbance of the samples at 217 nm.

TABLE 5. Parameters of the TSC models.

Parameter	Broadband light source	Narrowband tunable light source
R^2	0.9997	0.9996
RMSE	0.0069	0.0077
SSE	0.1531	0.1895

D. ESTABLISHMENT OF THE NITRATE CALCULATION MODEL

1) A NITRATE CALCULATION MODEL BASED ON THE BROADBAND LIGHT SOURCE SYSTEM

The TSC algorithm was used for the training set (seawater samples from Aoshan Bay, the Western Pacific, Sanggou Bay and the South China Sea with nitrate concentrations of 0-102 μmol/L). Afterwards, the calculation model based on the SVR algorithm was established to predict 380 testing samples. The ISUS algorithm was applied to the seawater data to make the comparison, which is shown in figure 9. The calculation model based on the data of 217-240 nm was established. The fitting function of the oligotrophic seawater absorbance by the ISUS algorithm can be expressed as [10]:

$$A = (A + B \times T) \times exp\left((C + D \times T) \times W\right) \quad (17)$$

where T is the sample temperature in deg C, and W is the wavelength minus 210 nm. The resultant regression parameters A, B, C, and D are 1.1500276, 0.02840, -0.3101349 and 0.001222, respectively. Since the predicted nitrate concentrations of the ISUS algorithm are notably linear with the reference nitrate concentrations, a linear correction to the ISUS values to obtain the final high accuracy values was derived and applied [30]. Figures 9 (a)-(c) show the prediction results of the TSC-SVR algorithm, (d)-(f) show the prediction results of the SVR algorithm, and (g)-(i) show the prediction results of the ISUS algorithm after linear correction. In (a), (d) and (g), the data of four seawater samples can be distributed around y = x, which indicates that different algorithms can well predict the seawater samples. (b), (e) and (h) show that the ISUS and SVR algorithms have large error ranges, while those calculated by the TSC-SVR algorithm are more concentrated at ± 2.5 μmol/L. From (c), (f) and (i), the SVR algorithm and ISUS algorithm have larger error ranges than the TSC-SVR algorithm. Moreover, with the TSC algorithm, the error range is reduced to ± 4 μmol/L, and the residuals are more concentrated at ± 2 μmol/L. Therefore, the TSC-SVR algorithm has the best prediction performance for the data based on the broadband light source system.

2) A NITRATE CALCULATION MODEL BASED ON THE NARROWBAND TUNABLE LIGHT SOURCE SYSTEM

After spectral preprocessing and TSC correction for the measurement data based on the narrowband tunable light source system, the calculation model is established to calculate the nitrate concentrations in testing seawater samples. The results are shown in figure 10, where (a)-(c) show the prediction results of the TSC-SVR algorithm, (d)-(f) show the prediction results of the SVR algorithm, and (g)-(i) show the prediction results of the ISUS algorithm after linear correction. Similar results are found for these testing samples

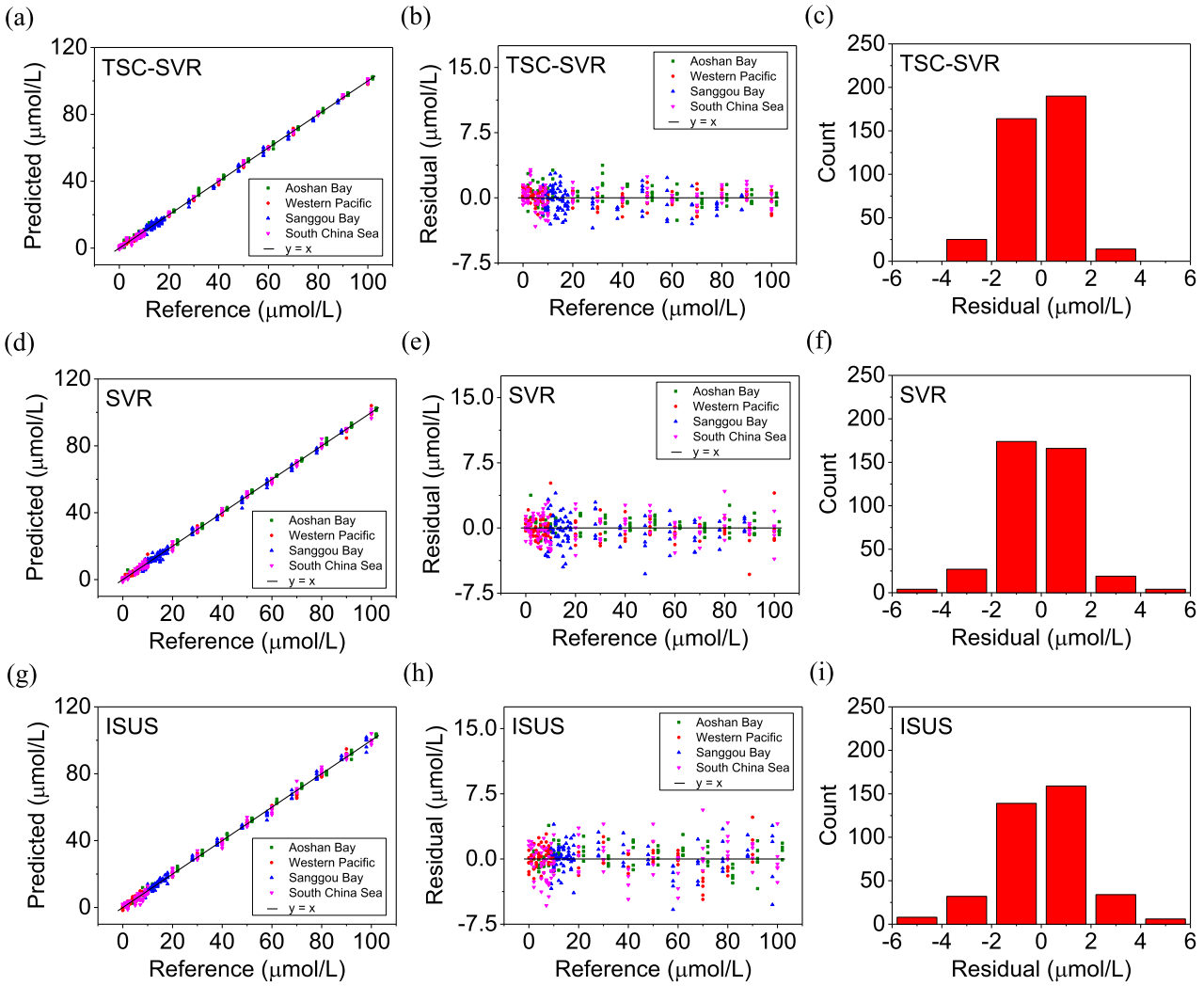

FIGURE 9. **Prediction results based on the broadband ultraviolet light source system. (a) Predicted nitrate concentrations of TSC-SVR algorithm versus reference concentrations; (b) residuals of TSC-SVR algorithm; (c) histogram plots of the residuals of TSC-SVR algorithm; (d) predicted nitrate concentrations of SVR algorithm versus reference concentrations; (e) residuals of SVR algorithm; (f) histogram plots of the residuals of SVR algorithm; (g) predicted nitrate concentrations of ISUS algorithm versus reference concentrations; (h) residuals of ISUS algorithm; (i) histogram plots of the residuals of ISUS algorithm.**

in figure 10. Furthermore, the SVR-based algorithm has much smaller residuals than the ISUS algorithm with an error range of ±4 μmol/L. From (c) and (f), we see that with the TSC algorithm, the residuals are further reduced, and the error range is basically ±2 μmol/L.

The parameters of different algorithms are shown and compared in Table 6. The experimental results show that the SVR-based algorithms has better prediction performance than the ISUS algorithm, including a smaller RMSE, a higher R^2 and a smaller error range. Table 6 shows that based on the SVR model, the narrowband tunable light source system obtained better prediction results than the broadband light source system. For the SVR algorithm, the RMSE and R^2 of the narrowband light source system are improved from 1.40 to 1.06 μmol/L (by 24.28%) and from 0.9980 to 0.9989, respectively, and the measurement error range is reduced from [−5.34, 5.16] to [−4.03, 3.01] μmol/L compared with the results of the broadband light source system. For the TSC-SVR algorithm, the RMSE and R^2 of the narrowband light source system are improved from 1.20 to 0.85 μmol (by 29.16%) and from 0.9985 to 0.9993, respectively, and the measurement error range is reduced from [−3.47,4.57] to [−3.01,2.99] μmol/L compared with the results of the broadband light source system. For the SVR-based results of the broadband ultraviolet light source system, the RMSE is reduced from 1.40 to 1.20 μmol/L using the TSC algorithm. For the results of the narrowband light source system, the RMSE is reduced from 1.06 to 0.85 μmol/L using the TSC algorithm. Therefore, the TSC correction algorithm can effectively increase the prediction accuracy of nitrate. Based on the ISUS algorithm, the broadband light source system has better prediction results than the narrowband light source

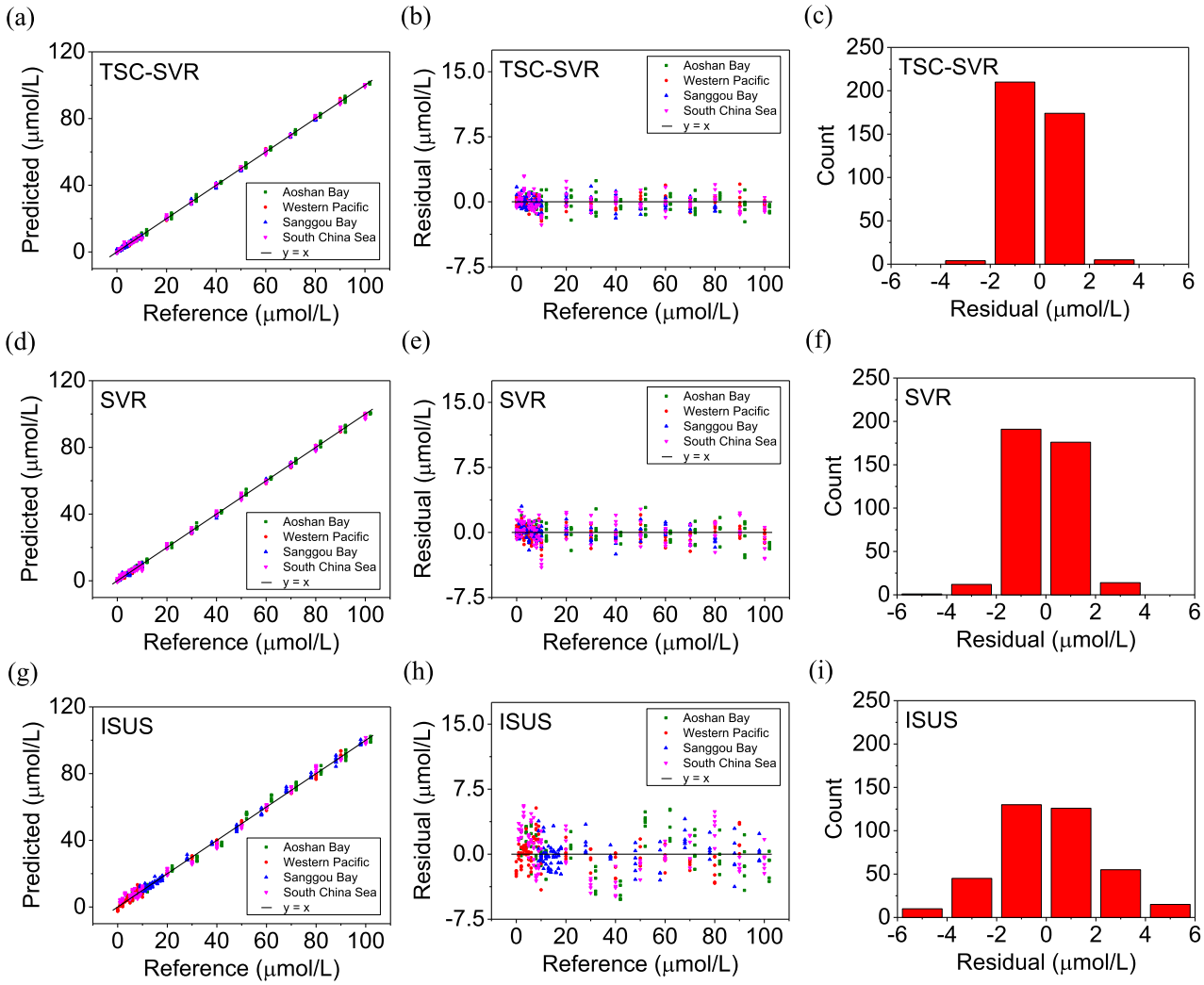

FIGURE 10. Prediction results based on the narrowband tunable light source system. (a) Predicted nitrate concentrations of TSC-SVR algorithm versus reference concentrations; (b) residuals of TSC-SVR algorithm; (c) histogram plots of the residuals of TSC-SVR algorithm; (d) predicted nitrate concentrations of SVR algorithm versus reference concentrations; (e) residuals of SVR algorithm; (f) histogram plots of the residuals of SVR algorithm; (g) predicted nitrate concentrations of ISUS algorithm versus reference concentrations; (h) residuals of ISUS algorithm; (i) histogram plots of the residuals of ISUS algorithm.

TABLE 6. Comparison of different model parameters.

Algorithm model		R^2	RMSE	Error range (μmol/L)
Broadband	SVR	0.9980	1.40	[-5.34, 5.16]
	TSC-SVR	0.9985	1.20	[-3.47,4.57]
	ISUS	0.9966	1.83	[-5.82,5.65]
Narrowband	SVR	0.9989	1.06	[-4.03, 3.01]
	TSC-SVR	0.9993	0.85	[-3.01,2.99]
	ISUS	0.9954	2.12	[-5.22,5.61]

system, but the error range remains large. The SVR algorithm uses multiple independent variables for regression, which can well separate the overlapping spectral data. In conclusion, the proposed method based on the narrowband tunable light source system and TSC-SVR algorithm has the best prediction performance.

A comparison of the results with the existing literature is shown in Table 7. Nitrate was measured based on UV spectroscopy in previous [18], [49]–[52]. In [18] and [50], SUNA (Satlantic Inc., USA) was used to measure nitrate in different water samples. With a larger measurement range, the error range will increase. In [49], the final nitrate calculation model was established based on the absorbance at 220 nm and 275 nm, since organic matter and nitrate do not have a strong absorption effect at a wavelength of 220 nm, while nitrate does not have an absorption effect at 275 nm. Therefore, the absorption at 275 nm is used to compensate for the nitrate at 220 nm. The detection range was 1-10 mg-N/L, and the error range was [-22, 34.28] μmol/L. In [51], the absorbance at 302 nm was used to calculate the nitrate content. In [52], scientists measured nitrate in turbidity water samples. After smoothing the spectrum, turbidity compensation was obtained, and the partial least squares (PLS)

TABLE 7. Comparison of different methods for measuring nitrate in water samples.

Reference	Detection range (mg N/L)	R^2	Error range (μmol/L)
[18]	0.33–22.2	-	[-49.28, 18.57]
[49]	1-10		[-22, 34.28]
[50]	0-10	0.976	[-7.14, 2.85]
[51]	0-8.23	0.9941	[-23.53, 35.29]
This paper	0–1.43	0.9993	[-3.01,2.99]
[52]	0-0.82	0.9943	[-3.53, 10.7]

algorithm was performed to establish the calculation model. The detection range was 0-0.82 mg-N/L, and the error range was [-3.53, 10.7] μmol/L. References [49] and [51] show that when nitrate is measured based on a single wavelength or two wavelengths of absorbance, the error range is relatively large. When it is measured based on a multi-wavelength spectrum, the measurement error range is smaller with a similar detection range. Therefore, with more spectral information, the multi-wavelength spectrum demonstrates better measurement performance than single-wavelength or two-wavelength absorbance. Compared with the results in the existing literature, the proposed method has the highest R^2 value and smallest error range. Therefore, the proposed method has better performance for nitrate measurement in water samples and can directly obtain the final results without further correction.

The temperature and salinity dependency of the residuals based on the narrowband light source system is calculated. The results are shown in figure 11, where (a) and (b) are the results of Aoshan Bay seawater, (c) and (d) are the results of Western Pacific seawater, (e) and (f) are the results of Sanggou Bay seawater, and (g) and (h) are the results of South China Sea water. Figure 11 shows that there is no obvious temperature or salinity dependency for the sample residuals.

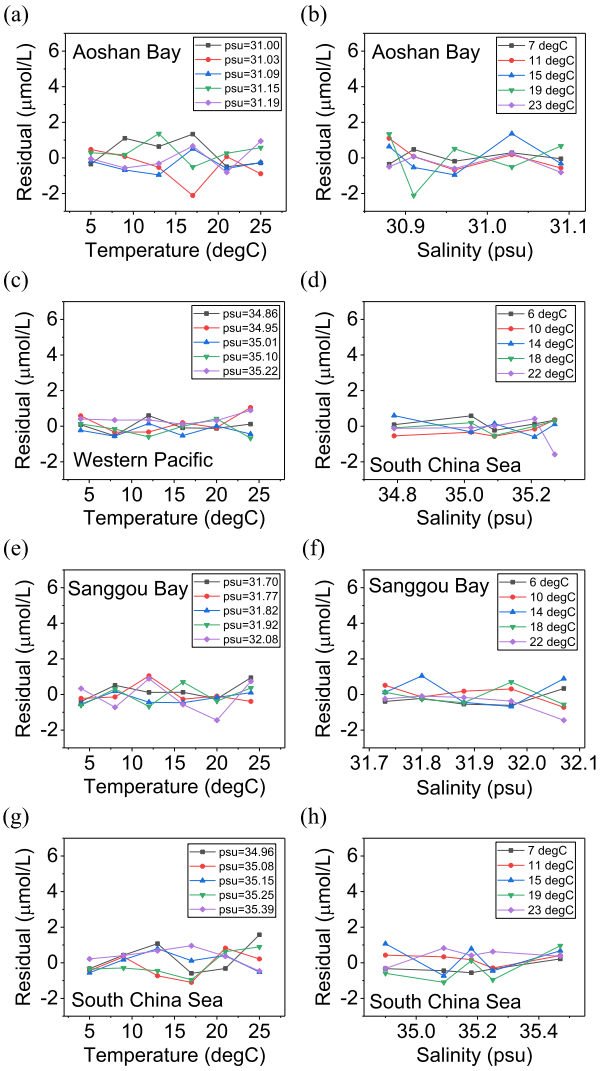

FIGURE 11. Temperature and salinity dependency results. (a)-(b) Temperature and salinity dependency of Aoshan Bay seawater; (c)-(d) temperature and salinity dependency of Western Pacific seawater; (e)-(f) temperature and salinity dependency of Sanggou Bay seawater; (g)-(h) temperature and salinity dependency of South China Sea water.

V. DISCUSSION

When using an ultraviolet spectrometer to determine the nitrate concentration in seawater, interference by other substances in the seawater, such as bromide and organic matter, occurs [53]. The absorbance values of seawater from Aoshan Bay (Qingdao, China), the Western Pacific, Sanggou Bay (Weihai, China), and the South China Sea at 217 nm were measured in the temperature range of 4-25 °C. These seawater samples have similar absorbance change trends to bromine ions, which is consistent with the results in previous investigations [53]. Since the nitrate concentration in Western Pacific seawater is less than 0.1 μmol/L, the TSC correction algorithm based on Western Pacific seawater is established based on a previous study [10] to reduce the influence of temperature and salinity on nitrate measurements.

The calculation results of different seawater samples are compared and analyzed by different models based on the SVR algorithm. Since we only measured the seawater samples in the laboratory, the influence of depth was not considered. For both the broadband light source system and narrowband light source system, the TSC-SVR algorithm has better prediction performance than the SVR without the TSC algorithm, and this conclusion is consistent with [10]. The reason is that the accuracy of nitrate prediction is improved when the spectral signal due to bromide is removed from the fit [9], which shows the effectiveness of the TSC algorithm. When calculating based on the same algorithm (SVR or TSC-SVR), the residuals based on the data obtained by the narrowband light source system are smaller than those of the broadband light source system, which indicates that the narrowband light source system can be applied to nitrate measurements with better performance. In conclusion, the narrowband light source system with the TSC-SVR algorithm demonstrates the best prediction performance with the largest R^2 value and lowest RMSE, which can be used to predict

nitrate concentrations in different sea areas. However, the SVR algorithm cannot self-learn. If the concentration exceeds the concentration range of the calculation model, then the accuracy will differ [35].

The measurement errors might come from several sources. First, bending of optical fibers in the operation process might cause a variation in absorbance, which will introduce a measurement error. Therefore, all optical fibers should remain straight and fixed to avoid this error. Second, it is necessary to remeasure I_D and $I_{\lambda,0}$ after the light source is turned on each time, since the light intensity will slightly fluctuate, and this drift of the lamp output is not a constant proportion at each wavelength [10]. Third, the presence of bubbles and biofouling in the probe will also affect the measured light intensity. The spectral error caused by this situation does not shift the baseline by a constant amount, which results in measurement error. Therefore, the probe condition should be handled in time to obtain accurate data.

The uncertainty of nitrate measurements using this approach greatly depends on the composition of the sampled water. Therefore, the uncertainty can be further reduced by processing absorbance spectra using additional information such as temperature, salinity, turbidity, CDOM and pressure [54]. In addition to temperature and salinity, CDOM has a certain absorbance in the ultraviolet wavelength range. In open and coastal oceans, the absorption spectrum of CDOM can be compensated by using a simple linear regression in the wavelength range for nitrate calculation [16]. Therefore, in this paper, the CDOM value is corrected based on a linear regression model after TSC correction to reduce the uncertainty. Other researchers also use additional information to process the data to obtain better results. For example, Sakamoto *et al.* studied the absorbance characteristics of seawater at different temperatures. The results show a clear reduction in measurement uncertainty when considering the influence of temperature, salinity and CDOM [10]. Zielinski *et al.* also found that the uncertainty decreased in turbid costal water measurements when considering temperature, salinity, turbidity and CDOM [16]. In addition, during deep-sea measurements, the pressure affects the nitrate measurement results. The results also show a reduction in uncertainty after the pressure has been considered in a deep-sea high-pressure environment [55].

The accuracy and sensitivity of the instrument are the key factors to accurately and rapidly detect nitrate. Therefore, future work will center on accuracy and sensitivity improvement. Since all seawater samples were filtered using a 0.45 μm filter membrane in this study, the influence of suspended particle matter (SPM) on the nitrate measurement was removed. However, for coastal sea water, the turbidity effect is an issue. Therefore, a turbidity correction algorithm will be studied to improve the detection precision of the system. To establish a real-time detection system and ensure its calculation speed, spectral data in the range of 212-240 nm are directly used for calculation without applying the feature extraction method, which simplifies the calculation model. However, an appropriate feature selection method will be considered in future optimized algorithms to improve the accuracy. Furthermore, a UV narrowband filter with better monochromaticity will be designed to cooperate with the photomultiplier (PMT) to improve the sensitivity of the system.

VI. CONCLUSION

A novel method to measure nitrate in seawater based on a narrowband tunable light source and an SVR-based algorithm has been proposed in this paper, which can realize real-time data acquisition and accurate calculation of nitrate concentrations. The DUV light source module was designed based on the wavelength-tunable principle of the interference filter. The parameters of the ultraviolet filters were calibrated, and the relationship between rotational angle and transmission wavelength of each filter was determined. The TSC algorithm based on LNS data was established in the temperature range of 4-25 °C, and the nitrate calculation model was established based on the SVR algorithm. The results show that based on the system with a narrowband tunable light source, the TSC-SVR algorithm demonstrates the best prediction results with an RMSE of 0.85 μmol/L and an error range from -3.01 to 2.99 μmol/L, which verify the advantages of the proposed method. This method has pollution-free, real-time measurements and high accuracy, which lays the foundation for in situ and accurate nitrate measurements.

ACKNOWLEDGMENT

(Xingyue Zhu and Kaixiong Yu contributed equally to this work.)

REFERENCES

[1] M. Saito, S.-I. Onodera, K. Miyaoka, J. Chen, M. Taniguchi, G. Liu, and Y. Fukushima, "Nitrate contamination in groundwater of the yellow river delta and its effect on the marine environment," *IAHS Publ.*, vol. 314, pp. 271–277, Jul. 2007.

[2] J. Ruzicka and E. H. Hansen, "Flow injection analyses—Part I. A new concept of fast continuous flow analysis," *Anal. Chim. Acta.*, vol. 78, no. 1, pp. 145–157, Aug. 1975.

[3] K. S. Johnson and R. L. Petty, "Determination of nitrate and nitrite in seawater by flow injection analysis," *Limnol. Oceanogr.*, vol. 28, no. 6, pp. 1260–1266, Nov. 1983.

[4] D. Thouron, R. Vuillemin, X. Philippon, A. Lourenço, C. Provost, A. Cruzado, and V. Garçon, "An autonomous nutrient analyzer for oceanic long-term *in situ* biogeochemical monitoring," *Anal. Chem.*, vol. 75, no. 11, pp. 2601–2609, Jun. 2003.

[5] M. Hajimorad, S. Alhloul, H. Mustafa, M. So, and H. Oswal, "Application of polypyrrole-based selective electrodes in electrochemical impedance spectroscopy to determine nitrate concentration," in *Proc. IEEE Sensors*, Oct. 2016, pp. 1–3.

[6] M. E. E. Alahi, A. Nag, S. C. Mukhopadhyay, and L. Burkitt, "A temperature-compensated graphene sensor for nitrate monitoring in real-time application," *Sens. Actuators A, Phys.*, vol. 269, pp. 79–90, Jan. 2018.

[7] N. Ağca, S. Karanlık, and B. Ödemiş, "Assessment of ammonium, nitrate, phosphate, and heavy metal pollution in groundwater from amik plain, southern Turkey," *Environ. Monitor. Assessment*, vol. 186, no. 9, pp. 5921–5934, Sep. 2014.

[8] M. S. Finch, D. J. Hydes, C. H. Clayson, B. Weigl, J. Dakin, and P. Gwilliam, "A low power ultra violet spectrophotometer for measurement of nitrate in seawater: Introduction, calibration and initial sea trials," *Analytica Chim. Acta*, vol. 377, nos. 2–3, pp. 167–177, Dec. 1998.

[9] K. S. Johnson and L. J. Coletti, "*In situ* ultraviolet spectrophotometry for high resolution and long-term monitoring of nitrate, bromide and bisulfide in the ocean," *Deep Sea Res. I, Oceanographic Res. Papers*, vol. 49, no. 7, pp. 1291–1305, Jul. 2002.

[10] C. M. Sakamoto, K. S. Johnson, and L. J. Coletti, "Improved algorithm for the computation of nitrate concentrations in seawater using an *in situ* ultraviolet spectrophotometer," *Limnol. Oceanography, Methods*, vol. 7, no. 1, pp. 132–143, Jan. 2009.

[11] R. Pidcock, M. Srokosz, J. Allen, M. Hartman, S. Painter, M. Mowlem, D. Hydes, and A. Martin, "A novel integration of an ultraviolet nitrate sensor on board a towed vehicle for mapping open-ocean submesoscale nitrate variability," *J. Atmos. Ocean. Technol.*, vol. 27, no. 8, pp. 1410–1416, Aug. 2010.

[12] G. Maclntyre, B. Plache, M. R. Lewis, J. Andrea, S. Feener, S. D. McLean, K. S. Johnson, L. J. Coletti, and H. W. Jannasch, "ISUS/SUNA nitrate measurements in networked ocean observing systems," presented at the Oceans, Oct. 2009. [Online]. Available: https://ieeexplore.ieee.org/stamp/stamp.jsp?arnumber=5422251

[13] D. Poornima, R. Shanthi, R. Ranith, L. Senthilnathan, R. K. Sarangi, T. Thangaradjou, and P. Chauhan, "Application of *in-situ* sensors (SUNA and thermal logger) in fine tuning the nitrate model of the bay of Bengal," *Remote Sens. Appl., Soc. Environ.*, vol. 4, pp. 9–17, Oct. 2016.

[14] J. Pan, F. Yu, Q. Ren, C. Wei, and J. Li, "Reliability analysis of spatial and temporal nitrate variations estimated by SUNA in the South Yellow Sea," *Mar. Sci.*, vol. 41, no. 12, pp. 9–16, Mar. 2017.

[15] R. D. Prien and D. J. Hydes, "A full ocean depth UV-spectrophotometer for nitrate measurements," presented at the OCEANS, Sep. 2003. [Online]. Available: https://ieeexplore.ieee.org/document/1282292

[16] O. Zielinski, D. Voß, B. Saworski, B. Fiedler, and A. Körtzinger, "Computation of nitrate concentrations in turbid coastal waters using an *in situ* ultraviolet spectrophotometer," *J. Sea Res.*, vol. 65, no. 4, pp. 456–460, May 2011.

[17] A. G. Rozin and M. W. Clark, "A comparison of analytical laboratory and optical *in situ* methods for the measurement of nitrate in north Florida water bodies," *Amer. Geophys. Union.*, vol. 2013, Dec. 2013, Art. no. H53H.

[18] T. T. Snazelle. (2015). *Results From Laboratory and Field Testing of Nitrate Measuring Spectrophotometers*. [Online]. Available: https://pubs.usgs.gov/of/2015/1065/pdf/ofr2015-1065.pdf

[19] X. Sun, Y. Bi, H. Karami, S. Naini, S. S. Band, and A. Mosavi, "Hybrid model of support vector regression and fruitfly optimization algorithm for predicting ski-jump spillway scour geometry," *Eng. Appl. Comput. Fluid Mech.*, vol. 15, no. 1, pp. 272–291, Jan. 2021.

[20] R. Taghizadeh-Mehrjardi, K. Schmidt, N. Toomanian, B. Heung, T. Behrens, A. Mosavi, S. S. Band, A. Amirian-Chakan, A. Fathabadi, and T. Scholten, "Improving the spatial prediction of soil salinity in arid regions using wavelet transformation and support vector regression models," *Geoderma*, vol. 383, Feb. 2021, Art. no. 114793.

[21] S. Shamshirband, F. Esmaeilbeiki, D. Zarehaghi, M. Neyshabouri, S. Samadianfard, M. A. Ghorbani, A. Mosavi, N. Nabipour, and K.-W. Chau, "Comparative analysis of hybrid models of firefly optimization algorithm with support vector machines and multilayer perceptron for predicting soil temperature at different depths," *Eng. Appl. Comput. Fluid Mech.*, vol. 14, no. 1, pp. 939–953, Jan. 2020.

[22] S. Shamshirband, A. Mosavi, T. Rabczuk, N. Nabipour, and K.-W. Chau, "Prediction of significant wave height; comparison between nested grid numerical model, and machine learning models of artificial neural networks, extreme learning and support vector machines," *Eng. Appl. Comput. Fluid Mech.*, vol. 14, no. 1, pp. 805–817, Jan. 2020.

[23] K. Yu, W. Liu, and D. X. Huang, "Characteristics analysis and stack design of angle-tuned filter," *Acta Photonica Sinica*, vol. 37, no. 6, pp. 1175–1179, Jun. 2008.

[24] M. R. Wang, K. Zhong, C. Liu, D. G. Xu, Y. Y. Wang, W. Shi, and J. Q. Yao, "Analyzing terahertz time-domain transmission spectra with multi-beam interference principle," *Proc. SPIE*, vol. 10030, Nov. 2021, Art. no. 100301H1.

[25] K. X. Yu, X. Y. Zhu, and C. Wu, "Design and experiment of a tunable narrow-passband deep UV light source," *Opto-Electron. Eng.*, vol. 48, no. 8, Aug. 2021, Art. no. 210173.

[26] C. G. Parazzoli, R. B. Greegor, K. Li, B. E. C. Koltenbah, and M. Tanielian, "Experimental verification and simulation of negative index of refraction using Snell's law," *Phys. Rev. Lett.*, vol. 90, no. 10, Mar. 2003, Art. no. 107401.

[27] K. Yu, Z. Ji, D. Huang, J. Yin, and J. Bao, "Design for the angle tuning system based on the thin-film filter," *J. Optoelectron.-Laser*, vol. 22, no. 10, pp. 65–68, Oct. 2011.

[28] F. Liu and X. Liu, "The study on the use of multi-level microstep control of a 2-phase hybrid stepping motor," *Micromotors Servo Technique*, vol. 40, no. 1, pp. 14–17, Jan. 2007.

[29] O. Zielinski, B. Fiedler, R. Heuermann, K. Arne, E. Kopiske, G. Meinecke, and K. Munderloh, "A new nitrate continuous observation sensor for autonomous sub-surface applications: Technical design and first results," presented at the Oceans, Jun. 2007. [Online]. Available: https://ieeexplore.ieee.org/document/4302300

[30] X. Zhu, K. Yu, X. Zhu, J. Su, and C. Wu, "An improved algorithm for measuring nitrate concentrations in seawater based on deep-ultraviolet spectrophotometry: A case study of the aoshan bay seawater and western Pacific seawater," *Sensors*, vol. 21, no. 3, p. 965, Feb. 2021.

[31] A. M. Andrew, "An introduction to support vector machines and other kernel-based learning methods," *Kybernetes*, vol. 30, pp. 103–115, Feb. 2001.

[32] L. Xie, P. W. Jie, and S. X. Yang, "A support vector machine discriminator for tobacco growing areas based on near-infrared spectrum," presented at IEEE Int. Conf., Aug. 2012. [Online]. Available: https://ieeexplore.ieee.org/stamp/stamp.jsp?tp=&arnumber=6308164

[33] X. Tan, F. Yu, and X. Zhao, "Support vector machine algorithm for artificial intelligence optimization," *Cluster Comput.*, vol. 22, no. S6, pp. 15015–15021, Nov. 2019.

[34] A. Gretton, A. Doucet, R. Herbrich, P. Rayner, and B. Olkopf, "Support vector regression for black-box system identification," presented at the IEEE Int. Conf. Robot. Automat. Singapore, Aug. 2002. [Online]. Available: https://ieeexplore.ieee.org/document/955292

[35] S. Hossain, C. W. K. Chow, G. A. Hewa, D. Cook, and M. Harris, "Spectrophotometric online detection of drinking water disinfectant: A machine learning approach," *Sensors*, vol. 20, no. 22, p. 6671, Nov. 2020.

[36] H. Song, Y. Xue, and L. Zhang, "Research on kernel function selection simulation based on SVM classification," *Comput. Modernization*, vol. 8, pp. 133–136, Aug. 2011.

[37] Z. Wang, L. Yao, Y. Cai, and J. Zhang, "Mahalanobis semi-supervised mapping and beetle antennae search based support vector machine for wind turbine rolling bearings fault diagnosis," *Renew. Energy*, vol. 155, pp. 1312–1327, Aug. 2020.

[38] L. Ma, "Semi-supervised regression based on particle swarm optimization and support vector machine," *Electron. Sci. Tech.*, vol. 26, pp. 10–13, Sep. 2013.

[39] M. A. Hariri-Ardebili and F. Pourkamali-Anaraki, "Support vector machine based reliability analysis of concrete dams," *Soil Dyn. Earthq. Eng.*, vol. 104, pp. 276–295, Jan. 2018.

[40] C. C. Chang and C. J. Lin, "LIBSVM: A library for support vector machines," *ACM Trans. Intell. Syst. Technol.*, vol. 2, no. 3, pp. 1–27, 2011.

[41] B. Liu and K. Li, "iPromoter-2L2.0: Identifying promoters and their types by combining smoothing cutting window algorithm and sequence-based features," *Mol. Therapy Nucleic Acids*, vol. 18, pp. 80–87, Dec. 2019.

[42] X. J. Zhu, C. Q. Feng, H. Y. Lai, W. Chen, and L. Hao, "Predicting protein structural classes for low-similarity sequences by evaluating different features," *Knowl.-Based Syst.*, vol. 163, pp. 787–793, Jan. 2019.

[43] Y. Wang, F. Shi, L. Cao, N. Dey, Q. Wu, A. S. Ashour, R. S. Sherratt, V. Rajinikanth, and L. Wu, "Morphological segmentation analysis and texture-based support vector machines classification on mice liver fibrosis microscopic images," *Curr. Bioinform.*, vol. 14, no. 4, pp. 289–294, Jan. 2018.

[44] N. Ogura and T. Hanya, "Nature of ultra-violet absorption in sea water," *Nature*, vol. 212, p. 758, Nov. 1966.

[45] V. D. Noto and M. Mecozzi, "Determination of seawater salinity by ultraviolet spectroscopic measurements," *Appl. Spectrosc.*, vol. 51, no. 9, pp. 1294–1302, Sep. 1997.

[46] J. Mack and J. R. Bolton, "Photochemistry of nitrite and nitrate in aqueous solution: A review," *J. Photochemistry Photobiol. A, Chem.*, vol. 128, nos. 1–3, pp. 1–13, Nov. 1999.

[47] A. W. Morris and J. P. Riley, "The bromide/chlorinity and sulphate/chlorinity ratio in sea water," *Deep Sea Res. Oceanographic Abstr.*, vol. 13, no. 4, pp. 699–705, Aug. 1966.

[48] W. Bao, X. Liu, and Z. Hao, "The narrow and broad senses on the salinity scale," *Acta Oceanol. Sinica*, vol. 20, pp. 77–83, Mar. 2001.

[49] X. Wu, R. Tong, Y. Wang, C. Mei, and Q. Li, "Study on an online detection method for ground water quality and instrument design," *Sensors*, vol. 19, no. 9, p. 2153, May 2019.

[50] L. Snyder, J. D. Potter, and W. H. McDowell, "An evaluation of nitrate, fDOM, and turbidity sensors in new hampshire streams," *Water Resour. Res.*, vol. 54, no. 3, pp. 2466–2479, Mar. 2018.

[51] Y. C. Moo, M. Z. Matjafri, H. S. Lim, and C. H. Tan, "New development of optical fibre sensor for determination of nitrate and nitrite in water," *Optik*, vol. 127, no. 3, pp. 1312–1319, Feb. 2016.
[52] X. Chen, G. Yin, N. Zhao, T. Gan, R. Yang, and W. Zhu, "Study on the determination of nitrate with UV first derivative spectrum under turbidity interference," *Spectrosc. Spectral Anal.*, vol. 39, no. 9, pp. 2912–2916, Nov. 2019.
[53] D. Meyer, R. D. Prien, L. Rautmann, M. Pallentin, J. J. Waniek, and D. E. Schulz-Bull, "*In situ* determination of nitrate and hydrogen sulfide in the Baltic sea using an ultraviolet spectrophotometer," *Frontiers Mar. Sci.*, vol. 5, pp. 1–10, Nov. 2018.
[54] R. D. Prien, "Optical assessment of nutrients in seawater," in *Woodhead Publishing Series in Electronic and Optical Materials, Subsea Optics and Imaging*. Sawston, U.K.: Woodhead Publishing, 2013, pp. 119–133.
[55] C. M. Sakamoto, K. S. Johnson, L. J. Coletti, and H. W. Jannasch, "Pressure correction for the computation of nitrate concentrations in seawater using an *in situ* ultraviolet spectrophotometer," *Limnol. Oceanography, Methods*, vol. 15, no. 10, pp. 897–902, Oct. 2017.

XINGYUE ZHU received the B.S. degree in optical information science and technology and the Ph.D. degree in optical engineering from the Nanjing University of Aeronautics and Astronautics, Nanjing, in 2012 and 2018, respectively.

From 2016 to 2017, she was a Visiting Scholar with Purdue University, USA. Since 2018, she has been a Postdoctoral Researcher with the Institute of Marine Science and Technology, Shandong University, Shandong. She has published 20 articles. Her research interests include high precision optical sensor design, data processing, and marine sensor applications.

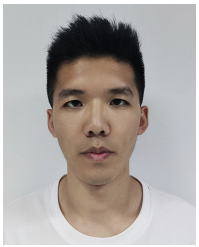

KAIXIONG YU received the B.S. degree in optoelectronic information science and engineering from the Changchun University of Science and Technology, China, in 2019. He is currently pursuing the master's degree with the Institute of Marine Science and Technology, Shandong University, China. His research interests include optical sensor design, system control, and data processing.

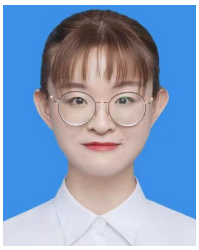

XIAOFAN ZHU received the B.S. degree in mechanical design manufacture and automation from the China University of Mining and Technology, China, in 2017, and the M.S. degree in electronic science and technology from Shandong University, China, in 2020. She has published two articles. Her research interests include sensor automation and data processing.

CHI WU received the Ph.D. degree in electrical and computer engineering from the University of Toronto, Canada. He is currently a Chair Professor and the Director of the Shandong Provincial Center for in-situ Marine Sensors, Institute of Marine Science and Technology, Shandong University, Qingdao, China. He was a Principal Investigator and the Senior Scientist with the NASA-Jet Propulsion Laboratory, California Institute of Technology, Pasadena, CA, USA; a Senior Scientist and the Project Leader with the Advanced Technology Laboratory, Nortel Networks, Ottawa, Canada; and the Founder of Kotura Inc., Monterey Park, CA, USA, a pioneering company in silicon photonics development and commercialization. His current research interests include marine sensors and the IoT sensors.